

Constant-overhead quantum error correction with thin planar connectivity

Maxime A. Tremblay,¹ Nicolas Delfosse,² and Michael E. Beverland²

¹*Institut quantique & Département de physique, Université de Sherbrooke, Sherbrooke, Qc, Canada, J1K 2R1*

²*Microsoft Quantum & Microsoft Research, Redmond, WA 98052, USA*

Quantum LDPC codes may provide a path to build low-overhead fault-tolerant quantum computers. However, as general LDPC codes lack geometric constraints, naïve layouts couple many distant qubits with crossing connections which could be hard to build in hardware and could result in performance-degrading crosstalk. We propose a 2D layout for quantum LDPC codes by decomposing their Tanner graphs into a small number of planar layers. Each layer contains long-range connections which do not cross. For any CSS code with a degree- δ Tanner graph, we design stabilizer measurement circuits with depth at most $(2\delta + 2)$ using at most $\lceil \delta/2 \rceil$ layers. We observe a circuit-noise threshold of 0.28% for a positive-rate code family using 49 physical qubits per logical qubit. For a physical error rate of 10^{-4} , this family reaches a logical error rate of 10^{-15} using fourteen times fewer physical qubits than the surface code.

Quantum error correction (QEC) is typically implemented by measuring Pauli operators called *stabilizer generators* of a QEC code to detect faults. In quantum low density parity check (LDPC) codes, the stabilizer generators have low weight, making them easier to implement than general codes. A further appealing property possessed by some quantum LDPC codes is *positive-rate*, allowing them to achieve arbitrarily low logical error rates with a constant ratio of tens of physical qubits per logical qubit. For large computations, this can correspond to more than an order of magnitude lower qubit overhead than alternative codes with vanishing rate such as the surface code. However, these positive-rate LDPC codes have non-local stabilizer generators [1, 2] making them somewhat daunting to implement in hardware. In this work, we seek a practical implementation of positive-rate quantum LDPC codes which performs well in a full circuit-level noise analysis.

To clarify our discussion, we define the *connectivity graph* of a quantum circuit, with vertices corresponding to qubits and edges connecting vertices corresponding to qubits which undergo entangling operations in the circuit. We can further define a *layout* as a specification of the physical locations of the connectivity graph's qubits and connections. In this paper we are interested in circuits which measure the stabilizer generators of a QEC code. Given a family of codes, we focus on constant-depth stabilizer measurement circuits to avoid a build-up of errors which could spoil any fault-tolerance threshold.

A natural first question is if the non-local stabilizer generators of positive-rate quantum LDPC codes can be measured using a circuit with local connectivity in a 2D qubit layout. In recent work [3], we show that although a single non-local stabilizer can be measured in constant depth, the full set of stabilizer generators cannot be collectively measured in constant depth without the ratio of logical to physical qubits vanishing.

Given that a 2D qubit layout with local connectivity is excluded for positive-rate quantum LDPC codes, we consider quantum hardware equipped with some set of long-

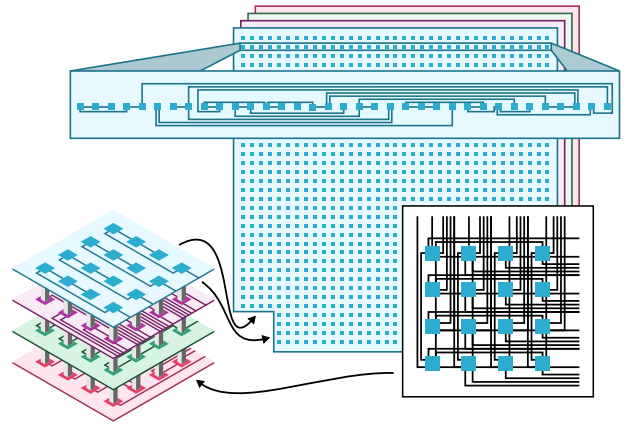


Figure 1. A crossing-free planar layout for hypergraph product codes with four layers. Stabilizer generators are measured using circuits built from single-qubit operations and CNOT gates between qubits connected by an edge. The top two layers have edges connecting qubits in the same row as shown in the zoom, while the lower two layers have edges connecting qubits in the same column. Each layer is planar, such that no pair of edges cross. For comparison, the lower right box shows the non-planar connections passing through the lower-left corner before the decomposition, which exhibits many crossings.

range connections. With unrestricted connections, one could simply lay out the code qubits in a 2D grid along with an ancilla for each stabilizer generator that has connections to the code qubits in that stabilizer's support. However, this typically results in an unbounded number of crossing connections [4, 5]; see Fig. 1. In many hardware platforms, in addition to being challenging to implement, crossing connections can spread error through crosstalk [6–9]. This raises the following question.

Can we construct high-threshold constant-depth stabilizer measurement circuits for positive-rate quantum LDPC codes in a 2D qubit layout without crossings in the two-qubit gate connectivity?

In this work, we provide a positive answer to this ques-

tion through the design of an l -planar layout, consisting of qubits placed in a 2D grid, with edges separated into $l = O(1)$ planar layers, with no crossings in each layer; see Figure 1. Furthermore, we provide a circuit construction consistent with this layered planar architecture to measure the stabilizer generators of any CSS-type [10, 11] quantum LDPC code in constant depth.

Theorem 1. Let Q be a CSS code such that each stabilizer generator has weight at most δ and each qubit is involved in at most δ stabilizer generators. Then, one can implement the measurement of all the stabilizer generators of Q with a circuit with depth $2\delta + 2$ using a $\lceil \delta/2 \rceil$ -planar layout.

Below, after proving this theorem, we refine these results by specializing to a family of quantum codes known as hypergraph product (HGP) codes [12] which are constructed from a pair of input graphs. In this case, we find a low-depth stabilizer measurement circuit which reduces to the standard circuit in the case of surface codes¹ [13]. Moreover, we prove in Lemma 1 that the circuit depth can be reduced to $\delta + 2$ when the vertices of the input graphs of the HGP code admit a balanced ordering.

Lastly, we numerically explore the performance of these circuits for a family of HGP codes using the decoding routine of Gropellier and Krishna [14], but replacing their idealized noise model by circuit noise. Using our layered planar connectivity, we obtain a circuit-noise threshold of $2.8(2) \times 10^{-3}$, providing strong evidence that these codes can offer a significant advantage over surface codes which have a comparable threshold.

Quantum LDPC codes — All the quantum codes we consider in this work are CSS codes [10, 11]. Recall that a CSS code with length n is defined by a set of commuting stabilizer generators $s_{X,1}, \dots, s_{X,r_X}, s_{Z,1}, \dots, s_{Z,r_Z}$ with $s_{X,i} \in \{I, X\}^n$ and $s_{Z,j} \in \{I, Z\}^n$. The X Tanner graph is the bipartite graph $T_X = (V, E)$ whose vertex set is $V = V_q \cup V_X$ where $V_q = \{q_1, \dots, q_n\}$ is the qubit set and $V_X = \{s_{X,1}, \dots, s_{X,r_X}\}$. There is an edge between q_i and $s_{X,j}$ iff $s_{X,j}$ acts non-trivially on qubit q_i . The Z Tanner graph T_Z is defined similarly from the Z stabilizer generators, and the overall Tanner graph is their union $T = T_X \cup T_Z$. The code is a quantum LDPC code if the Tanner graph has bounded degree. Quantum error correction works by measuring all the stabilizer generators and applying a correction based on the outcomes observed. Our goal is to design practical stabilizer measurement circuits for quantum LDPC codes.

We first show that quantum circuits with a low-degree connectivity graph can be implemented with a layered planar connectivity using a small number of layers. This

result applies to any quantum circuit (not just stabilizer measurement circuits) and in particular to all low-depth quantum circuits.

Proposition 1. Let C be a circuit made with single-qubit and two-qubit operations whose connectivity graph has degree at most δ . Then, C can be implemented with a $\lceil \delta/2 \rceil$ -planar layout.

Proof. This follows directly from the fact that for any graph with degree at most δ , the smallest edge partition such that each subgraph is planar involves at most $\lceil \delta/2 \rceil$ subgraphs [15, 16]. Furthermore, since any planar graph can be drawn with arbitrary vertex location [17], we can fix the position of each qubit across layers. \square

We now introduce the *coloration circuit* associated with an edge coloration of a Tanner graph that can be used for any CSS code. An *edge coloration* of a graph is a coloration of the edges such that incident edges support distinct colors. We will often consider a *minimum edge coloration*, that is an edge coloration with a minimum number of colors.

Algorithm 1: Coloration circuit

input : A minimum edge coloration \mathcal{C}_X of T_X .

output: The measurement outcome of all X stabilizer generators.

- 1 Prepare an ancilla in $|+\rangle$ for each generator $s_{X,i}$.
 - 2 **for** color $c \in \mathcal{C}_X$ **do**
 - 3 Simultaneously apply all gates $\text{CNOT}_{i \rightarrow j}$ from the i th ancilla to the j th data qubit supported on an edge $\{i, j\}$ with color c .
 - 4 Measure each ancilla in the X basis.
-

Proposition 2. Let Q be a CSS code with X Tanner graph T_X . Then, the coloration circuit measures all the X stabilizer generators of Q in depth $\deg(T_X) + 2$.

Proof. The CNOTs applied in step 3 can be applied simultaneously because they correspond to edges with the same color, guaranteeing they have disjoint support. We see the circuit measures the X generators by rearranging the CNOTs, which commute, to form a sequence of single-generator measurement circuits. Each such circuit prepares an ancilla in $|+\rangle$, applies CNOTs from the ancilla to the generator's support, then measures the ancilla in the X basis. The depth of the coloration circuit is $\deg(T_X) + 2$ because the Tanner graph, which is bipartite, admits an edge coloration with $\deg(T_X)$ colors [18]. \square

Swapping the roles of X and Z provides a Z stabilizer measurement circuit with depth $\deg(T_Z) + 2$. We are now equipped to prove Th. 1.

Proof of Th. 1. By Proposition 2, a circuit extracting both X and Z syndromes with depth $\deg(T_X) +$

¹ Surface codes are HGP codes formed when the input graphs are the Tanner graphs of a pair of repetition codes

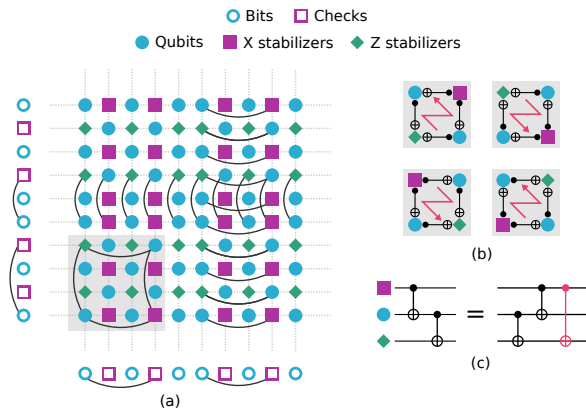


Figure 2. (a) The Tanner graph of a HGP code is the Cartesian product of two bipartite input graphs. Here qubits are displayed according to their label, which does not correspond to their physical location in the 2D layout. (b) The four possible configurations in which an X and a Z stabilizer can overlap. Red arrows show the cardinal circuit ordering. (c) The commutation of a pair of CNOT gates.

$\deg(T_Z) + 2$ is formed by running the X then the Z circuit with two overlapping time steps. The connectivity graph of the cardinal circuit has degree $\deg(T)$. Therefore Prop. 1 proves the existence of a $\lceil \deg(T)/2 \rceil$ -planar layout. \square

For some codes, the depth can be further reduced by interleaving X and Z stabilizer measurements. However, the design of an interleaved X/Z stabilizer measurement circuit is non-trivial because the CNOT gates involved in X and Z measurements do not commute. Now we specialize to HGP codes for which we provide an interleaved X/Z stabilizer measurement circuit.

Hypergraph product codes — The HGP code $\text{HGP}(G_1, G_2)$ [12] is defined from the Cartesian product $G_1 \times G_2$ of two bipartite graphs (Fig. 2(a)). For $m \in \{1, 2\}$, let $V_m = B_m \cup C_m$ be the vertex set of G_m and E_m be its edge set. Edges of E_m connect a vertex of B_m with a vertex of C_m . We assume that each vertex of G_m is given by a label $i = 1, \dots, |V_m|$. Each pair $(i, j) \in B_1 \times B_2 \cup C_1 \times C_2$ represents a data qubit of the HGP code while each pair (i, j) in $B_1 \times C_2$ (resp. $C_1 \times B_2$) corresponds to an X (resp. Z) stabilizer generator. The stabilizer generator with label (i, j) , denoted $S_{(i,j)}$ is supported on the qubits with label (i', j) where $\{i', i\} \in E_1$ and (i, j') with $\{j, j'\} \in E_2$. To avoid confusion with the coordinates introduced later which specify the physical locations of qubits in a 2D layout, we refer to the pair (i, j) as a *data qubit label* or *stabilizer generator label*.

We associate a *direction* $\mathbf{N}, \mathbf{S}, \mathbf{E}, \mathbf{W}$ with each edge. An edge between stabilizer vertex (i, j) and qubit vertex (i', j') with $j' = j + \ell \pmod{|V_1|}$ has direction \mathbf{N} if $0 < \ell \leq |V_1|/2$ and direction \mathbf{S} otherwise. We define the

directions \mathbf{E} and \mathbf{W} similarly for edges between stabilizer and qubit vertices (i, j) and (i', j) . For each direction $\mathbf{D} \in \{\mathbf{N}, \mathbf{S}, \mathbf{E}, \mathbf{W}\}$, we consider the subgraph $T_{\mathbf{D}}$ of the Tanner graph T induced by the edges with direction \mathbf{D} .

The following circuit interleaves X and Z measurements and can achieve a depth lower than the coloration circuit.

Algorithm 2: Cardinal circuit

- input** : A minimum edge coloration $\mathcal{C}_{\mathbf{D}}$ of $T_{\mathbf{D}}$.
output: The outcome of the measurement of all the X and Z stabilizer generators.
- 1 Prepare an ancilla in $|+\rangle$ for each X stabilizer generator and an ancilla in $|0\rangle$ for each Z stabilizer generator.
 - 2 **for** *direction* $\mathbf{D} \in \{\mathbf{E}, \mathbf{N}, \mathbf{S}, \mathbf{W}\}$ **do**
 - 3 **for** *color* $c \in \mathcal{C}_{\mathbf{D}}$ **do**
 - 4 Simultaneously apply all CNOT gates supported on an edge of $T_{\mathbf{D}}$ with color c .
 - 5 Measure each X and Z ancilla in the X and Z basis respectively.
-

Note that the CNOT is either aligned or anti-aligned with an edge depending on the type of the stabilizer. The control qubit of the CNOT is the ancilla for X stabilizers, and it is the data qubit for Z stabilizers.

Proposition 3. Let Q be a hypergraph product code with Tanner graph T . Then, the cardinal circuit implements the measurement of all the stabilizer generators of Q in depth $\deg(T_{\mathbf{N}}) + \deg(T_{\mathbf{S}}) + \deg(T_{\mathbf{E}}) + \deg(T_{\mathbf{W}}) + 2$.

Proof. It is easy to check that the depth of the cardinal circuit is $\deg(T_{\mathbf{N}}) + \deg(T_{\mathbf{S}}) + \deg(T_{\mathbf{E}}) + \deg(T_{\mathbf{W}}) + 2$. This is because the bipartite graph $T_{\mathbf{D}}$ admits an edge coloration with $\deg(T_{\mathbf{D}})$ colors [18].

We now prove by induction that the cardinal circuit measures the stabilizer generators. Denote by C_m the circuit obtained by applying the cardinal circuit construction to the subset of stabilizer generators s_1, \dots, s_m . Clearly, for $m = 1$, the circuit $C(s_1)$ measures the stabilizer generator s_1 . We will show that the concatenation of C_m and $C(s_{m+1})$, that we denote $C_m C(s_{m+1})$, has the same action as C_{m+1} .

If all the CNOT gates of $C(s_{m+1})$ commute with all the CNOTs of C_m , we can simply reorder the CNOTs of the circuit $C_m C(s_{m+1})$ to obtain the cardinal circuit C_{m+1} . Assume now that some CNOT gates of $C(s_{m+1})$ do not commute with the gates of C_m . Again, we would like to put the CNOT of $C_m C(s_{m+1})$ in the cardinal order, but swapping these CNOTs produces extra CNOTs as one can see in Fig. 2(d). We will show that these extra CNOTs cancel out.

If s_{m+1} is a Z stabilizer, the corresponding CNOTs only fail to commute with CNOTs associated with the previous X stabilizer generators s_i that overlap with s_{m+1} . Swapping these CNOTs produces an extra gate

$\text{CNOT}_{s_i \rightarrow s_{m+1}}$ as shown in Fig. 2(c). By the hypergraph product construction, if s_{m+1} overlaps with an X stabilizer generator s_i , their overlap contains exactly two qubits, in one of the four possible configurations of Fig. 2(b). To bring the CNOTs into cardinal order, we need to perform either 0 or 2 swaps between the CNOTs of s_{m+1} and s_i . This results in two consecutive CNOT gates $\text{CNOT}(s_i, s_{m+1})$ which cancel out. Thus, reordering the CNOT gates in $C_m C(s_{m+1})$ to produce C_{m+1} preserves the action of the circuit. A similar argument applies when s_{m+1} is an X stabilizer generator. Applying this inductively starting with a single stabilizer generator, we reach the cardinally ordered circuit proving that it has the same action as the initial stabilizer measurement circuit. \square

From Prop. 3 we see that the cardinal circuit only has a lower depth than the coloration circuit if the Tanner subgraphs T_D have sufficiently low degree. To ensure this, we must order the vertices (i, j) of the Tanner graph to distribute the edges more equally between the four directions around each vertex. This motivates the notion of balanced ordering that we introduce now.

A *balanced ordering* for a graph $G = (V, E)$ is a labeling of the vertices by integers $i = 1, \dots, |V|$ such that for each vertex i we have $\delta_+(i) - \delta_-(i) = (\delta(i) \bmod 2)$ where $\delta_+(i)$ is the number of vertices connected to i of the form $(i + \ell) \pmod{|V|}$ with $0 < \ell \leq |V|/2$ and $\delta_-(i) = \delta(i) - \delta_+(i)$. When the graph is not clear from the context, we will use the notation $\delta_{\pm}(G, i) = \delta_{\pm}(i)$. The following lemma is proven in the Supplemental Material.

Lemma 1. Let $Q = \text{HGP}(G_1, G_2)$ be a hypergraph product code. Then, we have

$$\deg(T) \leq \sum_{\mathbf{D}=\mathbf{N},\mathbf{S},\mathbf{E},\mathbf{W}} \deg(T_{\mathbf{D}}) \leq 2 \deg(T).$$

Moreover, if G_1 and G_2 have only even degree vertices and admit a balanced ordering, then the lower bound is tight.

For HGP codes based on even, balanced graphs, this lemma, combined with Prop. 3, proves that the depth of the cardinal circuit is about half that of the coloration circuit.

Numerical results — We use the standard circuit noise model. We simulate the performance of a family of HGP codes with parameters $[[25s^2, s^2]]$, *i.e.* encoding $k = s^2$ logical qubits into $n = 25s^2$ physical qubits. The syndrome extraction is performed with the cardinal circuit using $24s^2$ ancilla qubits. More details about the noise model and the codes can be found in the Supplementary Material.

To decode and correct faults, we use the approach set out in Ref. [19], which is based on Belief Propagation (BP) [20, 21] and Small Set Flip (SSF) [22]. After each round of stabilizer extraction, BP is iterated until there

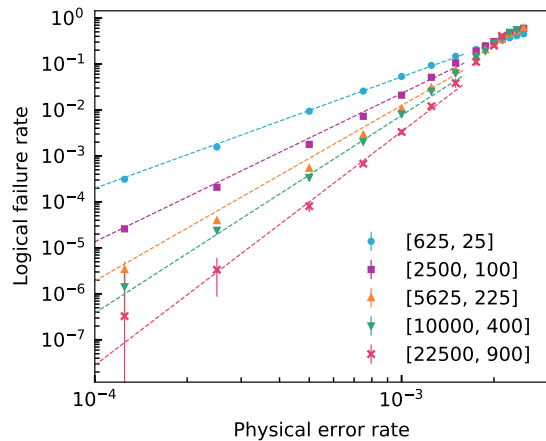


Figure 3. The failure rate per round averaged over 10 successive rounds of error correction. The dashed lines are obtained using $P_L(p, k) = c_1(p/p_t)^{c_2 k^{c_3}}$ finding fitting constants $c_1 = 0.64$, $c_2 = 1.3$, $c_3 = 0.21$ and the threshold $p_t = 2.8(2) \times 10^{-3}$.

is a local minimum of the number of violated stabilizer measurements. To probe the overall performance after T rounds of error correction, a perfect stabilizer measurement round is applied and BP and SSF are alternated until the SSF decoder converges to a correction. If either no correction is found, or if the net effect of all noise and corrections is to introduce a logical operator, we say that a failure has occurred by round T .

By sampling over many realizations of this procedure with outcomes extracted using the cardinal circuit, we estimate the logical failure rate of a family of HGP codes over a range of physical failure rates as shown in Fig. 3. We use a simple extrapolation of the data to estimate a threshold of $p_t = 2.8(2) \times 10^{-3}$ and compare the qubit overhead with that of the surface code in Table I. Based on our simulation, we propose the heuristic formula

$$P_L(p, k) = c_1(p/p_t)^{c_2 k^{c_3}} \quad (1)$$

where $c_1 = 0.64$, $c_2 = 1.3$, $c_3 = 0.21$ and $k = 24s^2$ to provide an estimate of the logical failure rate per round with physical error rate $p < p_t$. Further details on the code construction and our numerical approach can be found in the Supplementary Material.

Outlook and hardware challenges — We have shown that syndrome extraction can be implemented in constant depth using a planar layout for any CSS quantum LDPC code, including HGP codes, but also many other families of interest including hyperbolic codes [24] and homological product codes [25]. Our design simultaneously seeks to minimize the depth of the stabilizer measurement circuit which achieves faster quantum error correction and reduce the time allowed for error buildup, while also avoiding crossings of the connections that cou-

Logical failure rate	10^{-9}	10^{-12}	10^{-15}
Logical qubits	1600	6400	18 496
Surface code physical qubits	387 200	2 880 000	13 354 112
HGP code physical qubits	78 400	313 600	906 304
Improvement using HGP codes	$4.94\times$	$9.18\times$	$14.73\times$

Table I. Total number of data and ancilla qubits required to achieve specific logical failure rates with a physical error rate of 10^{-4} using surface codes and HGP codes. The HGP code data is estimated from Eq. 1, while the surface code data is estimated using the formula $P'_L(p, k, d) = ak(p/p'_t)^{(d+1)/2}$ with optimistic values of $p'_t = 0.011$ and $a = 0.03$ from Ref. [13] and Ref. [23].

ple qubits which is expected to improve fabrication and reduce cross-talk. Further improvements could come from optimizing the circuit to minimize the spreading of errors [26] using better decoders [27–30], or by leveraging improved planar graph algorithms.

We hope that these significant quantum error-correction advantages will motivate experimental teams to overcome the challenges to build quantum hardware in planar layouts. We foresee two major obstacles. Firstly, our design requires a number of long range links within each layer. Significant experimental progress has been made in that direction using for instance photonic couplings to establish long range connections [31–38] but it is unclear which of these approaches could be scaled to larger systems. Secondly, there is a tension between the need for insulation between the layers to reduce crosstalk and the fact that data qubits must participate in all layers.

Acknowledgments — The authors would like to thank David Poulin for his encouragements in the early stage of this project, Jeongwan Haah for his comments on a preliminary version of this work and Nouédyn Baspin for insightful discussions.

SUPPLEMENTAL MATERIAL

Tanner subgraphs for HGP codes

Here we prove the bound stated in Lemma 1 on the degree of sub graphs of the Tanner graphs of HGP codes.

Proof. Edges of the Tanner graph of the form $\{(i, j), (i', j)\}$ are called *horizontal edges* and the edges $\{(i, j), (i, j')\}$ are *vertical edges*. The lower bound is trivial because the four types of edges form a partition of the edge set of T . Consider the subgraph $T_{\mathbf{h}}$ (resp. $T_{\mathbf{v}}$) of T induced by horizontal (resp. vertical) edges. By definition, $T_{\mathbf{E}}$ and $T_{\mathbf{W}}$ are subgraphs of $T_{\mathbf{h}}$ which implies $\deg(T_{\mathbf{E}}), \deg(T_{\mathbf{W}}) \leq \deg(T_{\mathbf{h}})$. Similarly, we obtain $\deg(T_{\mathbf{S}}), \deg(T_{\mathbf{N}}) \leq \deg(T_{\mathbf{v}})$. More-

over, due the product structure of the graph, we have $\deg(T) = \deg(T_{\mathbf{h}}) + \deg(T_{\mathbf{v}})$, which leads to the upper bound.

Assume that G_1 and G_2 have only even degree vertices and are equipped with a balanced ordering and let us prove that the lower bound is tight. Then, we have $\delta_{\pm}(G_m, i) = \deg_{G_m}(i)/2$. Let (i, j) be a maximum degree vertex in $T_{\mathbf{N}}$. If (i, j) is a stabilizer vertex, then by definition of the direction \mathbf{N} , the degree of (i, j) in the graph $T_{\mathbf{N}}$ is given by $\delta_+(G_2, j)$. If (i, j) is a qubit vertex, its degree is given by $\delta_-(G_2, j)$. Therefore, we always have

$$\begin{aligned} \deg(T_{\mathbf{N}}) &\leq \max(\delta_+(G_2, j), \delta_-(G_2, j)) \\ &= \deg_{G_2}(j)/2 \\ &\leq \deg(G_2)/2. \end{aligned}$$

By the same reasoning, we obtain $\deg(T_{\mathbf{S}}) \leq \deg(G_2)/2$ and combining both equations, we find

$$\deg(T_{\mathbf{S}}) + \deg(T_{\mathbf{N}}) \leq \deg(G_2). \quad (2)$$

Applying the same argument to horizontal edges, we get

$$\deg(T_{\mathbf{E}}) + \deg(T_{\mathbf{W}}) \leq \deg(G_1). \quad (3)$$

Using Eq. (2) and (3), we obtain

$$\sum_{\mathbf{D}=\mathbf{N},\mathbf{S},\mathbf{E},\mathbf{W}} \deg(T_{\mathbf{D}}) \leq \deg(G_1) + \deg(G_2)$$

which concludes the proof of the lemma because $\deg(G_1) + \deg(G_2) = \deg(T)$. \square

Numerical simulations

In our numerical studies we consider HGP codes constructed from the product of random $(3, 4)$ -regular Tanner graphs with $4s$ bit nodes and $3s$ check nodes with girth at least 8. The codes are generated using the procedure of Ref. [19] and for each s , we pick the best code from a few hundred samples by decoding i.i.d noise with the SSF decoder. The actual number of samples is based on the decoding time and the computing resources. Depending on the code length, this ranges from 50 to 1000 samples. For all these graphs, we found a balanced vertex ordering using a greedy Metropolis-Hasting inspired algorithm by defining a measure of how close to balanced is a vertex ordering of a graph.

We use a circuit noise model in which each operation, including an identity gate, is faulty with probability p . If a unitary operation is faulty, we apply a random uniform non-trivial Pauli error on the support of the operation. If a single-qubit measurement is faulty, its outcome is flipped.

In our simulations, we estimate the logical failure rate by averaging over T successive rounds of error correction.

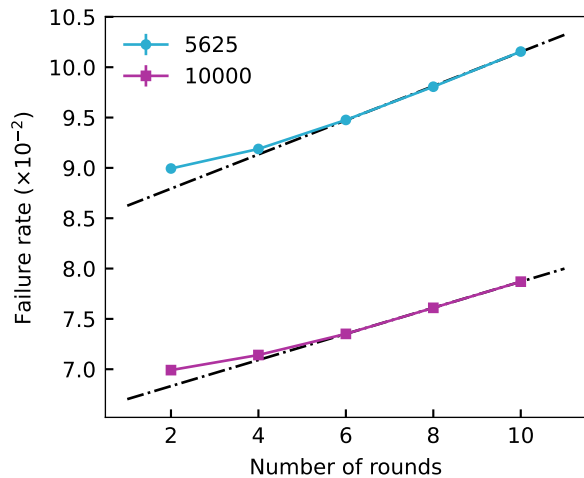


Figure 4. Failure rate after an increasing number of error correcting rounds for codes of length 5625 and 10000 with $p = 10^{-3}$. We observe that after 6 rounds, the increment per round is roughly constant.

Based on Fig. 4 we can assume that the logical error rate after T rounds behaves roughly like $P_L(T) = c + qT$ for some constants c and q that depend on the noise rate and the code. For simplicity, we estimate the logical error rate per round as $P_L = P_L(T)/T$ for $T = 10$ rounds of error correction. This value leads to a pessimistic estimate of the logical failure rate after T rounds for any $T \geq 10$. This is a reasonable model because we expect these code blocks to be kept alive for many logical cycles during a quantum computation because they encode hundreds of thousands of logical qubits. Indeed, one could conceivably run a full large scale quantum algorithm using only the logical qubits encoded in a single block of the codes simulated in Fig. 3.

-
- [1] S. Bravyi, D. Poulin, and B. Terhal, *Physical Review Letters* **104**, 050503 (2010), publisher: American Physical Society.
- [2] N. Baspin and A. Krishna, arXiv preprint arXiv:2109.10982 (2021).
- [3] N. Delfosse, M. E. Beverland, and M. A. Tremblay (2021), to appear.
- [4] M. Ajtai, V. Chvátal, M. M. Newborn, and E. Szemerédi, in *North-Holland Mathematics Studies*, Vol. 60 (Elsevier, 1982) pp. 9–12.
- [5] F. T. Leighton, *Complexity issues in VLSI: optimal layouts for the shuffle-exchange graph and other networks* (MIT press, 1983).
- [6] M. Sarovar, T. Proctor, K. Rudinger, K. Young, E. Nielsen, and R. Blume-Kohout, *Quantum* **4**, 321 (2020), publisher: Verein zur Förderung des Open Access Publizierens in den Quantenwissenschaften.
- [7] S. Debnath, N. M. Linke, C. Figgatt, K. A. Landsman, K. Wright, and C. Monroe, *Nature* **536**, 63 (2016), bandiera_abtest: a Cg_type: Nature Research Journals Number: 7614 Primary_atype: Research Publisher: Nature Publishing Group Subject_term: Optical manipulation and tweezers; Quantum information; Qubits Subject_term_id: optical-manipulation-and-tweezers; quantum-information; qubits.
- [8] C. Neill, P. Roushan, K. Kechedzhi, S. Boixo, S. V. Isakov, V. Smelyanskiy, A. Megrant, B. Chiaro, A. Dunsworth, K. Arya, R. Barends, B. Burkett, Y. Chen, Z. Chen, A. Fowler, B. Foxen, M. Giustina, R. Graff, E. Jeffrey, T. Huang, J. Kelly, P. Klimov, E. Lucero, J. Mutus, M. Neeley, C. Quintana, D. Sank, A. Vainsencher, J. Wenner, T. C. White, H. Neven, and J. M. Martinis, *Science* **360**, 195 (2018), publisher: American Association for the Advancement of Science.
- [9] A. Ash-Saki, M. Alam, and S. Ghosh, in *Proceedings of the ACM/IEEE International Symposium on Low Power Electronics and Design, ISLPED '20* (Association for Computing Machinery, New York, NY, USA, 2020) pp. 25–30.
- [10] A. R. Calderbank and P. W. Shor, *Physical Review A* **54**, 1098 (1996), publisher: American Physical Society.
- [11] A. M. Steane, *Physical Review A* **54**, 4741 (1996), publisher: American Physical Society.
- [12] J. Tillich and G. Zémor, *IEEE Transactions on Information Theory* **60**, 1193 (2014).
- [13] A. G. Fowler, M. Mariantoni, J. M. Martinis, and A. N. Cleland, *Physical Review A* **86**, 032324 (2012), publisher: American Physical Society.
- [14] A. Grospellier and A. Krishna, arXiv:1810.03681 [quant-ph] (2019).
- [15] J. H. Halton, *Information Sciences* **54**, 219 (1991).
- [16] P. Mutzel, T. Odenthal, and M. Scharbrodt, *Graphs and Combinatorics* **14**, 59 (1998).
- [17] J. Pach and R. Wenger, in *Graph Drawing, Lecture Notes in Computer Science*, edited by S. H. Whitesides (Springer, Berlin, Heidelberg, 1998) pp. 263–274.
- [18] N. Alon, *Information Processing Letters* **85**, 301 (2003).
- [19] A. Grospellier, L. Grouès, A. Krishna, and A. Leverrier, arXiv:2004.11199 [quant-ph] (2020).
- [20] R. Gallager, *IRE Transactions on Information Theory* **8**, 21 (1962), conference Name: IRE Transactions on Information Theory.
- [21] D. Poulin and Y. Chung, arXiv:0801.1241 [quant-ph] (2008), arXiv: 0801.1241.
- [22] A. Leverrier, J. Tillich, and G. Zémor, in *2015 IEEE 56th Annual Symposium on Foundations of Computer Science* (2015) pp. 810–824.
- [23] D. S. Wang, A. G. Fowler, and L. C. L. Hollenberg, *Physical Review A* **83**, 020302 (2011).
- [24] N. P. Breuckmann, C. Vuillot, E. Campbell, A. Krishna, and B. M. Terhal, *Quantum Science and Technology* **2**, 035007 (2017).
- [25] S. Bravyi and M. B. Hastings, in *Proceedings of the forty-sixth annual ACM symposium on Theory of computing* (2014) pp. 273–282.
- [26] N. P. Breuckmann and J. N. Eberhardt, arXiv preprint arXiv:2103.06309 (2021).
- [27] P. Panteleev and G. Kalachev, arXiv preprint arXiv:1904.02703 (2019).
- [28] J. Roffe, D. R. White, S. Burton, and E. T. Campbell, arXiv preprint arXiv:2005.07016 (2020).

- [29] N. Delfosse, V. Londe, and M. Beverland, arXiv preprint arXiv:2103.08049 (2021).
- [30] A. O. Quintavalle and E. T. Campbell, arXiv preprint arXiv:2105.02370 (2021).
- [31] L. Trifunovic, F. L. Pedrocchi, and D. Loss, *Physical Review X* **3**, 041023 (2013), publisher: American Physical Society.
- [32] C. Monroe, R. Raussendorf, A. Ruthven, K. Brown, P. Maunz, L.-M. Duan, and J. Kim, *Physical Review A* **89**, 022317 (2014).
- [33] N. H. Nickerson, J. F. Fitzsimons, and S. C. Benjamin, *Physical Review X* **4**, 041041 (2014).
- [34] G. Tosi, F. A. Mohiyaddin, V. Schmitt, S. Tenberg, R. Rahman, G. Klimeck, and A. Morello, *Nature Communications* **8**, 450 (2017), number: 1 Publisher: Nature Publishing Group.
- [35] W. W. Ho, C. Jonay, and T. H. Hsieh, *Physical Review A* **99**, 052332 (2019), publisher: American Physical Society.
- [36] K. J. Morse, R. J. Abraham, A. DeAbreu, C. Bowness, T. S. Richards, H. Riemann, N. V. Abrosimov, P. Becker, H.-J. Pohl, M. L. Thewalt, *et al.*, *Science advances* **3**, e1700930 (2017).
- [37] L. Bergeron, C. Chartrand, A. Kurkjian, K. Morse, H. Riemann, N. Abrosimov, P. Becker, H.-J. Pohl, M. Thewalt, and S. Simmons, *PRX Quantum* **1**, 020301 (2020).
- [38] A. Metelmann and H. Türeci, *Physical Review A* **97**, 043833 (2018).